Electronic Research Archive

https://www.aimspress.com/journal/era

ERA, 32(7): 4659–4683.
DOI: 10.3934/era.2024212
Received: 13 February 2024
Revised: 23 May 2024
Accepted: 05 June 2024
Published: 26 July 2024

Research article

A power generation accumulation-based adaptive chaotic differential evolution algorithm for wind turbine placement problems

Shi Wang*, Sheng Li and Hang Yu

College of Computer Science and Technology, Taizhou University, Taizhou, Jiangsu 225300, China

* **Correspondence:** Email: wangshi@tzu.edu.cn.

Abstract: The focus on clean energy has significantly increased in recent years, emphasizing eco-friendly sources like solar, wind, hydropower, geothermal, and biomass energy. Among these, wind energy, utilizing the kinetic energy from the wind, is distinguished by its economic competitiveness and environmental benefits, offering scalability and minimal operational emissions. It requires strategic turbine placement within wind farms to maximize energy conversion efficiency, a complex task involving the analysis of wind patterns, turbine spacing, and technology. This task has traditionally been tackled by meta-heuristic algorithms, which face challenges in balancing local exploitation with global exploration and integrating problem-specific knowledge into the search mechanism. To address these challenges, an innovative power generation accumulation-based adaptive chaotic differential evolution algorithm (ACDE) is proposed, enhancing the conventional differential evolution approach with an adaptive chaotic local search and a wind turbine adjustment strategy based on tournament selection. This strategy aimed to prioritize energy-efficient turbine positions and improve population diversity, thereby overcoming the limitations of existing meta-heuristic algorithms. Comprehensive experiments with varying wind rose configurations demonstrated ACDE's superior performance in energy conversion efficiency, showcasing its potential in optimizing wind turbine placement for enhanced clean energy production. The wind farm layout optimization competition hosted by the Genetic and Evolutionary Computation Conference provided a comprehensive set of complex wind farm layouts. This dataset was utilized to further validate the performance of the algorithms. The results unequivocally demonstrate the superiority of ACDE when tackling complex optimization problems.

Keywords: clean energy; meta-heuristic; differential evolution; artificial intelligence; wind turbine placement; power generation accumulation; adaptive; genetic algorithms

1. Introduction

In recent years, clean energy has garnered increasing attention. Often used interchangeably with "renewable energy", it denotes energy sources that are eco-friendly and do not emit greenhouse gases during their production or usage [1]. The defining feature of clean energy is its origin from natural, renewable sources that are self-replenishing and exert minimal environmental impact. Principal forms of clean energy encompass solar, wind, hydropower, geothermal, and biomass energy [2]. Transitioning to clean energy is pivotal in addressing climate change and diminishing our dependence on fossil fuels [3]. Technological advancements are enhancing the efficiency and affordability of these energy sources, thereby broadening their accessibility and global adoption [4]. This paradigm shift promises not only environmental advantages but also economic and social benefits, potentially spurring job creation in emerging sectors and reducing long-term energy costs [5, 6].

Wind energy, which harnesses kinetic energy from the wind, stands out among clean energy sources for its increasing attention and contrast to other forms such as solar, hydropower, geothermal, and biomass energy [7]. Although more intermittent and less predictable than geothermal energy, advancements in weather forecasting have improved its predictability, especially in areas with consistent wind patterns [8]. Wind farms require more land than solar farms for the same energy output, but this space can be used for other purposes, unlike the significant environmental and social impacts of hydropower plants [9]. Wind turbines demand more maintenance than solar panels due to their moving parts, yet this is often simpler than the maintenance required for biomass or hydropower plants [10].

Economically, wind energy is becoming more competitive, with rapidly decreasing costs and lower operational expenses compared to biomass and some hydropower installations [11]. Environmentally, it is one of the cleanest forms, with no greenhouse gas emissions during operation and minimal lifecycle emissions, primarily from manufacturing and installation [12]. Wind energy, adaptable from small turbines to large wind farms, is particularly well-suited for coastal and open plain areas, offering different scalability and location advantages compared to solar, hydropower, and geothermal energy [13].

The strategic placement of turbines in a wind farm is essential for maximizing the efficiency of wind energy conversion [14]. This intricate task involves the judicious positioning of turbines to enhance energy production while simultaneously reducing costs and environmental repercussions [15]. Managing the wind flow and the wake effect is crucial [16]. The wake from each turbine can decrease the efficiency of other turbines situated downwind, necessitating a thoughtful placement strategy to mitigate these effects [17]. The site's physical attributes, such as its topography and land availability, are pivotal in determining turbine placement, with an emphasis on harmonizing with the natural landscape and existing ecosystems [18].

Optimizing energy yield stands as a foremost objective, demanding an analysis of wind patterns, the spacing between turbines, and the employed technology [19]. The design process is an integration of various disciplines, encompassing engineering, environmental considerations, and economic factors. Frequently, this process leverages sophisticated computational models and optimization algorithms to ascertain the most effective turbine layout, a crucial determinant of the wind farm's operational efficiency and its sustainable future [20]. Meta-heuristic algorithms [21, 22] have been widely used to tackle the wind turbine placement problems [23, 24]. These methods include genetic algorithms [25,26], particle swarm optimization [27,28], differential evolution algorithms [29], spherical evolution [30], evolutionary algorithms [31, 32], reinforcement learning [33, 34], and hybrid algorithms [35].

However, existing meta-heuristic algorithms, which are commonly employed to address wind-related problems, typically encounter two significant challenges: 1) achieving a balance between local exploitation and global exploration during the search process [36–38], and 2) integrating problem-specific knowledge into the search mechanism [39–41]. The balance between local exploitation and global exploration is crucial in optimization algorithms, determining their effectiveness in finding optimal solutions [42]. Local exploitation focuses on intensively searching around promising solutions to find local optima, whereas global exploration aims to diversely search the broader solution space to uncover new regions [43, 44]. Striking an optimal balance between these strategies prevents the algorithm from getting trapped in local optima early on and ensures efficient exploration of the search space [45, 46]. On the other hand, incorporating problem-oriented knowledge into the search mechanism significantly enhances the efficiency and effectiveness of optimization algorithms by tailoring their search strategies to the specific characteristics of the problem at hand [47]. This approach involves integrating domain-specific heuristics, customizing the fitness function, seeding the initial population with promising solutions, and adapting search operators to exploit the structural properties of the problem domain [48–50]. Such customization allows algorithms to quickly identify and focus on promising areas of the search space, leading to faster convergence and the discovery of higher-quality solutions tailored to the unique demands of the problem [51–53].

Building on the motivation outlined above, we innovatively propose a power generation accumulation-based adaptive chaotic differential evolution algorithm (ACDE), specifically designed for optimizing wind turbine placement. This algorithm enhances the conventional differential evolution (DE) approach [54–57], a type of evolutionary algorithm renowned for its straightforward application and effectiveness in tackling optimization challenges characterized by non-linearity, indeterminacy, and multiple optima [58–61]. Our method integrates an adaptive chaotic local search into DE to boost its ability to exploit solutions. Additionally, we introduce a novel power generation accumulation-based tournament selection strategy. This strategy prioritizes previously selected positions with higher wind energy generation potential for future selection, while the least effective positions in the current generation are substituted with unplaced ones to enrich population diversity. Such enhancements address two major hurdles faced by existing meta-heuristic algorithms. To assess ACDE's efficacy, we conducted comprehensive experiments involving four distinct wind rose configurations with varying layout constraints. The comparative analysis with other leading-edge methods demonstrates that ACDE significantly surpasses its counterparts in energy conversion efficiency. The contributions of this work are listed as following:

1) In wind farm layout optimization problems, we introduce an adaptive chaotic differential evolution algorithm (ACDE) based on power generation accumulation. Convergence and stability analyses demonstrate that ACDE exhibits high robustness, ensuring the provision of high-quality solutions. We implement extensive experiments with five state-of-the-art algorithms to verify the performance of ACDE, which demonstrates the superiority of ACDE.
2) To enhance the performance of ACDE, we introduce a chaotic local search and a wind turbine adjustment strategy. The former improves the algorithm's exploitation ability, ensuring convergence, while the latter enhances population diversity, thereby improving exploration ability. Both strategies contribute significantly to the algorithm's effectiveness.
3) We explore the impact of parameters on the algorithm's performance under varying wind scenarios, aiming to identify an optimal parameter configuration that yields high-quality solutions.

Additionally, an ablation study validates the effectiveness of the proposed strategies.

2. Related work

The placement of wind turbines encompasses significant technical challenges, as highlighted in [16, 62]. Predicting and harnessing wind patterns accurately is complicated by varying terrain and the wake effect, wherein turbines can disrupt each other's airflow, leading to reduced efficiency. Optimal turbine spacing is pivotal to maximize energy output and efficient land use, while also mitigating the wake effect. Furthermore, the influence of terrain topography on placement decisions is profound. Hills, valleys, and other land forms significantly affect wind flow and turbine efficiency. These aspects, in tandem with the necessity for durable and maintainable installations, render wind turbine placement a complex and multi-dimensional technical issue. The wake effect [63] entails a decrease in wind speed and an increase in turbulence behind an operational turbine. This phenomenon, caused by the turbines extracting energy from the wind, results in slower and more turbulent air downstream, adversely affecting the efficiency of adjacent turbines through lower wind speeds and heightened mechanical stress. Therefore, managing the wake effect is vital for the optimal layout and performance of wind farms.

Optimizing the configuration of wind farms (WFO) revolves around the strategic placement of wind turbines to optimize power generation, mitigate expenses, and lessen environmental repercussions. At the heart of WFO challenges lies a primary goal: to minimize the cost-to-power output ratio of the wind farm. This objective necessitates fine-tuning the arrangement of turbines within the farm, denoted by Y, and the total turbine count, represented by M. The aggregate cost of construction is determined using a bespoke function, for instance, the one proposed by Mosetti [64], which accounts for the turbine count and their spatial distribution. The optimization endeavor also aims to amplify the farm's overall power production under a variety of wind conditions, effectively boiling down to power maximization given a constant turbine count. The power yield of each turbine is computed considering elements such as wind velocity, orientation, and the configuration Y. The efficiency of power generation within the farm is gauged by a conversion efficiency metric, reflecting the effectiveness of the turbine arrangement.

As aforementioned, a critical aspect in WFO is the wake effect, which describes the diminution in wind velocity and the shift in wind trajectory behind operational turbines, leading to reduced energy generation and accelerated degradation of turbines downstream. To quantify the wake's velocity and its influence on the power generation of adjacent turbines, models like the one by Jensen are employed [63]. These models are crucial in balancing various factors to devise an efficient and productive wind farm layout.

From a mathematical standpoint, the ambition of wind farm configuration optimization is to elevate the wind farm's power generation capabilities. The objective function is formulated as:

$$h = \text{minimize } \frac{C_{\text{total}}}{P_{\text{total}}} \tag{2.1}$$

where C_{total} represents the overall construction cost, and P_{total} denotes the total power output under differing wind scenarios. This task involves determining the optimal arrangement Y and the precise count of turbines M.

For computing the construction expense, a specific equation akin to Mosetti's is utilized, expressed

as:

$$C_{\text{total}} = M\left(\frac{2}{3} + \frac{1}{3}e^{-0.00174M^2}\right) \tag{2.2}$$

In scenarios where the turbine quantity is static, the primary goal simplifies to maximizing the farm's total power output under selected wind conditions ξ, shown as:

$$h(Y) = \text{maximize } P_{\text{total}} = \sum_{i=1}^{M} \sum_{v,\theta} p(v,\theta) Q_i(v,\theta,Y) \tag{2.3}$$

Here, $Q_i(v,\theta,Y)$ is the i-th turbine's power output given wind velocity v and direction θ in configuration Y, with $p(v,\theta)$ being the wind velocity and direction's probability distribution.

The farm's power generation efficiency is evaluated through a conversion efficiency η, i.e.,

$$\eta = \frac{P_{\text{total}}}{M \sum_{v,\theta} Q_r(v,\theta,Y) \cdot p(v,\theta)} \tag{2.4}$$

$Q_r(v,\theta,Y)$, disregarding wake effects, denotes the turbine's rated power under specific wind conditions v and θ. A superior η indicates a more effective turbine layout.

The wake effect, a pivotal factor, is characterized by a decline in wind velocity and directional shifts post-turbine, which impacts the wind speed and efficiency of downstream turbines within the same farm. To evaluate wake velocity, Jensen's model is employed, predicting wind speed reduction and heightened turbulence in the turbine's wake, envisaged as a cylindrical zone extending downstream from the turbine. This model provides insights into the wake's velocity deficit, aiding in the estimation of downstream turbines' power output and the farm's overall energy yield. Jensen's model, despite its simplicity, proves useful across various wind farm configurations.

Various meta-heuristic algorithms have been employed to address WFO. Among these, genetic algorithms stand out as the most notable and advanced. Grady et al. [65] utilized a genetic algorithm to enhance wind turbine placement for optimal power production, simultaneously reducing the number of turbines and land use across three wind conditions: unidirectional uniform wind, variable-direction uniform wind, and variable-direction non-uniform wind. This approach involved 600 individuals in 20 subpopulations, evolving through 2500 to 3000 generations to identify the best turbine configurations, focusing on metrics like fitness, total power output, and efficiency. The findings present unique insights compared to previous studies, with explanations for these variations. Yang et al. presented a refined genetic algorithm using Boolean coding to optimize turbine layouts in a 2-km-by-2-km wind farm, aiming for the lowest possible cost per power output under three wind scenarios. This method proved more cost-effective than prior optimizations, displaying exceptional convergence stability and efficiency, particularly in densely populated grid setups. Moreover, the algorithm's versatility is emphasized, indicating its suitability for a wide array of engineering optimization challenges. Abdelsalam et al. [66] proposed an optimization method for wind farm layouts using a binary real coded genetic algorithm combined with local search strategies, integrating a robust single wake model for precise wake interaction analysis. The algorithm differentiates turbine locations and power outputs, with local search further honing the quality of solutions. Significant improvements over earlier methods were achieved through the application of the Jensen wake model and sum of squares model for power estimation. Ju et al. [25] critiqued the traditional genetic algorithm for its propensity to yield suboptimal solutions

in wind farm layout optimization, owing to the limitations of its crossover and mutation stages. They introduced two innovative algorithms, the adaptive genetic algorithm (AGA) and self-informed genetic algorithm (SIGA), which incorporate self-adaptivity and awareness to detect and ameliorate inefficiencies in turbine positioning. These algorithms enhance optimization effectiveness by applying strategies such as AGA's random relocation and SIGA's information-guided relocation via a multivariate adaptive regression splines model. Lastly, Ju et al. [26] tackled the optimization of wind turbine layouts considering the wake effect, which diminishes efficiency, by proposing a novel support vector regression guided genetic algorithm (SUGGA). This method merged the self-adjustment capabilities inherent in natural evolution with support vector regression to optimize turbine placement, taking into account the landowners' willingness to lease their property for wind farms. Extensive simulations revealed this algorithm's superiority over conventional methods under diverse scenarios, providing valuable perspectives on landowner participation's effect on wind farm efficiency and land valuation for planning purposes. Nevertheless, these algorithms encounter challenges related to the imbalance between exploitation and exploration, along with inadequate leveraging of problem-specific knowledge in WFO. This situation drives us to propose a more efficient and effective optimization algorithm tailored for WFO.

3. Proposed ACDE

Researchers have significantly advanced various meta-heuristic algorithms aimed at enhancing the power conversion efficiency of wind farms. Concurrently, they have introduced variant operators to address the delicate balance between exploitation and exploration in WFO. The traditional DE method is an evolutionary algorithm celebrated for its simplicity and efficiency in addressing optimization problems marked by non-linearity, unpredictability, and the presence of multiple optimal solutions. However, these approaches still suffer from challenges related to low convergence performance and inadequate optimization efficiency. Hence, we propose a chaotic local search method based on the global best individual to expedite convergence. Recognizing that this approach may diminish population diversity, we further introduce a wind turbine adjustment strategy based on power generation accumulation for each individual. This strategy aims to enhance population diversity while maintaining convergence acceleration. It includes initialization, chaotic local search, mutation, crossover, and selection processes.

The population P is randomly generated within a boundary limitation,

$$\begin{aligned} &P = \{X_1, X_2, \cdots, X_i, \cdots, X_N\} \\ &X_i = \{x_i^1, x_i^2, \cdots, x_i^d, \cdots, x_i^D\} \\ &\text{s.t.} \quad x_l \le x_i^d \le x_u \end{aligned} \tag{3.1}$$

where X_i is the i-th individual in the population, x_i^d is the individual information of the d-th dimension, which is encoded into an integer-value number denoting the position of wind turbines in a wind farm. N means the number of individuals. Notably, a wind farm is constructed as a discrete model in this study. The wind farm is divided into several grids, and wind turbines are placed in the center of these grids. For example, a 12×12 wind farm consists of 144 positions where wind turbines are placed. However, to reduce the dimension of the problems, we employ integer encoding. In this way, the dimension of WFO becomes the number of wind turbines to reduce the difficulty. D denotes the dimension of the

optimization problems. In wind farm layout optimization, it represents the number of wind turbines. x_l and x_u are the lower and upper bound of the solution space, respectively.

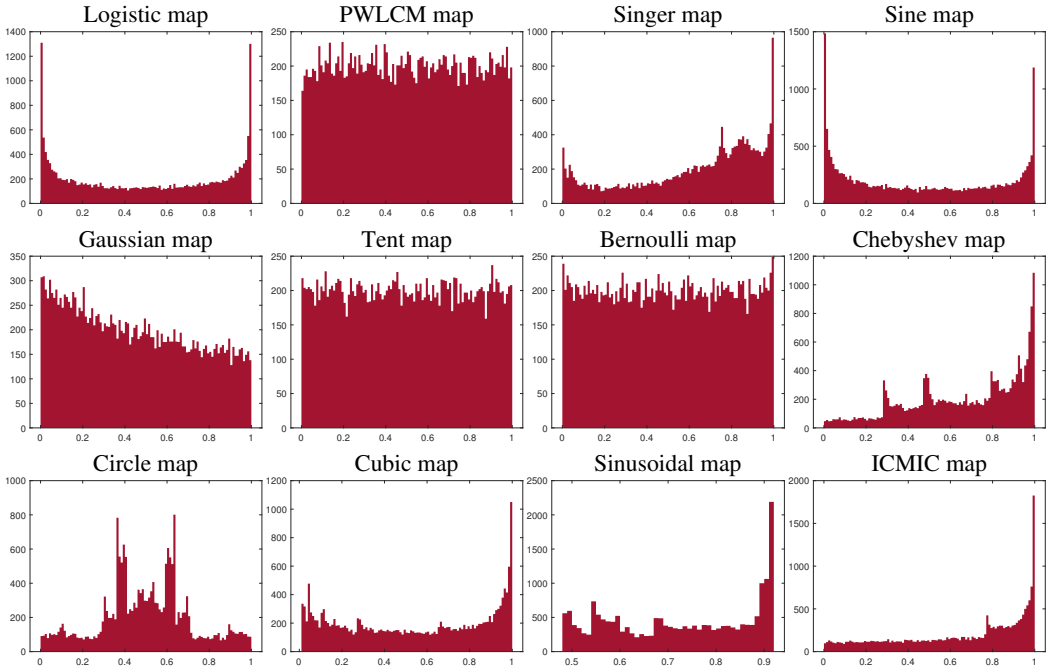

Figure 1. The illustration of chaotic maps.

Chaotic local search has been widely used in optimization algorithms to improve performance owing to its properties of ergodicity and randomicity [67–70]. ACDE utilizes twelve chaotic maps into the global best individual to improve the exploration ability. It is formulated by

$$X' = X_g + rad(x_u - x_l)(z_j - 0.5) \tag{3.2}$$

where X_g is the global best individual and *rad* is the hyper-parameter to control the scale of the chaotic local search. z_j represents the j-th ($j = 1, 2, ..., 12$) chaotic map. Building on insights from previous research [71–74], this study utilizes twelve unique chaotic maps as potential candidates: the logistic map, piecewise linear chaotic map, singer map, sine map, Gaussian map, tent map, Bernoulli map, Chebyshev map, circle map, cubic map, sinusoidal map, and the iterative chaotic map with infinite collapses. Their illustrations are shown in Figure 1. We propose a memory-based selection method for choosing the most appropriate chaotic map to facilitate chaotic localization. To track the performance of each chaotic map, two metrics are employed: the success count (S_j) and the failure count (F_j), which record the effectiveness of each map under selected conditions.

$$S_j = \begin{cases} S_j + 1, & \text{if } f(X') > f(X_g) \\ 0, & \text{otherwise} \end{cases} \tag{3.3}$$

$$F_j = \begin{cases} F_j + 1, & \text{if } f(X') \leq f(X_g) \\ 0, & \text{otherwise} \end{cases} \tag{3.4}$$

Then, the selection probability p_j^t of the chaotic maps is calculated depending on the counters,

$$\begin{aligned} Mp_j^t &= \frac{S_j}{S_j + F_j} + \epsilon \\ p_j^t &= \frac{Mp_j^t}{\sum_{j=1}^{J} Mp_j^t} \end{aligned} \tag{3.5}$$

where ϵ is a small number to ensure that each chaotic map has a probability of being selected to improve diversity.

Besides, an adaptive wind turbine adjustment strategy is proposed to improve the exploitation ability of the algorithm for wind farm layout optimization. It adaptively adjusts the position of wind turbines to improve the power generation. It utilizes the population information to maintain a set of promising positions. Then, a tournament selection is used to choose an unplaced position and move the wind turbine with the worst power generation into it.

$$x_i^{worst} = \text{tour}(L_u) \tag{3.6}$$

where tour$(\cdot)$ is the tournament selection. $10\%RL + N$ positions of a wind farm are chosen randomly to join the tournament, where the winner of the position with the best power generation replaces the worst one. L_u saves the potential of power generation of all of the position by population information. It accumulates the power generation of all positions,

$$\begin{aligned} L_u &= \{PG_1, PG_2, \cdots, PG_i, \cdots, PG_{RL}\} \\ PG_i &= \begin{cases} PG_i + g(x_j^d), & \text{if } x_j^d == i \\ PG_i, & \text{otherwise} \end{cases} \end{aligned} \tag{3.7}$$

where PG_i represents the power generation accumulation of the i-th position in the wind farm. When the i-th position is used to place a wind turbine, the power generation of the wind turbine is added to PG_i. $g(x_j^d)$ calculates the power generation of the d-th wind turbine in the i-th individual. RL is the maximum scale of the wind farm. It is set to $12 \times 12 = 144$ in this study.

The DE/current-to-best mutation operation is used to mutate the individuals,

$$V_i = X_i + F_i(X' - X_i) + F_i(X_{r1} - X_{r2}) \tag{3.8}$$

where X' is the best individual in the population after the chaotic search, and X_{r1} and X_{r2} are randomly chosen individuals from the population. F_i is the scale factor for the i-th individual. The crossover operation is described as follows:

$$u_i^d = \begin{cases} v_i^d, & \text{if } r < CR_i \text{ or } d = d_r \\ x_i^d, & \text{otherwise} \end{cases} \tag{3.9}$$

where r is a random number in the interval $(0, 1)$. CR_i is the crossover rate of the i-th individual and d_r is the random dimension to ensure the execution of the crossover operation. Finally, the selection operation selects the better individuals for the next generation,

$$X_i = \begin{cases} U_i, & \text{if } f(U_i) > f(X_i) \\ X_i, & \text{otherwise} \end{cases} \tag{3.10}$$

Furthermore, F and CR are two vital parameters to balance the exploration and exploitation. An adaptive parameter is implemented to update them,

$$\begin{aligned} F_i &= \text{randc}(\mu_F, 0.1) \\ \mu_F &= (1-c)\cdot\mu_F + c\cdot \text{mean}_\text{L}(S_F) \end{aligned} \tag{3.11}$$

where randc$(\cdot)$ means the Cauchy distribution. μ_F is the mean of the Cauchy distribution, which is initialized to be 0.5. c is a constant within $(0, 1)$, and S_F records all of the successful scale factors. $\text{mean}_\text{L}(\cdot)$ is the Lehmer mean. Similarly, the crossover rate is updated as follows:

$$\begin{aligned} CR_i &= \text{randn}(\mu_{CR}, 0.1) \\ \mu_{CR} &= (1-c)\cdot\mu_{CR} + c\cdot \text{mean}(S_{CR}) \end{aligned} \tag{3.12}$$

where randn$(\cdot)$ means the normal distribution. μ_{CR} is the mean of the normal distribution, which is initialized to be 0.5. S_{CR} records all of the successful crossover rates. The pseudo-code of ACDE is shown in Algorithm 1. Initially, the population is randomly generated and encoded using integer coding. Subsequently, J chaotic maps are created for a chaotic search. Following this, the chaotic search operation is applied to enhance the quality of the best individual. Simultaneously, success and failure memory are computed to guide the selection of chaotic maps for the next iteration. Afterward, a wind turbine adjustment strategy is implemented for all individuals to enhance population diversity. Finally, conventional DE operators, including mutation, crossover, and selection, are executed to generate offspring.

Algorithm 1: The pseudo-code of ACDE.

Input : Population size $N = 120$, $iter = 0$, $MaxIter = 200$
for *i = 1:N* **do**
  Randomly initializing population P.
  Evaluating each individual of population $f(X_i)$ by Eq (2.4).
end
Selecting the best individual X_g from P.
Generating chaotic maps $Z = \{z_1, z_2, ..., z_J\}$.
while $iter < MaxIter$ **do**
  Chaotic Local Search for X_g by Eq (3.2).
  Updating the success rate of chaotic maps by Eqs (3.3)–(3.5).
  for *i=1:N* **do**
    Using the wind turbine adjustment strategy to update individuals by Eqs (3.6)–(3.7).
    Mutation and crossover operations of individuals by Eqs (3.8) and (3.9).
    Updation of F and CR by Eqs (3.11) and (3.12).
  end
end
Output: Y, η, P_{total}

4. Experimental results and discussions

To evaluate the effectiveness of ACDE, we carried out extensive testing across four different wind rose patterns, each with its own set of layout restrictions. Figure 2 shows four wind rose diagrams, each representing different wind scenarios. A wind rose is a graphical tool used to display the distribution of wind speeds and directions. Wind scenario 1 displays a dominant wind direction from approximately 225 degrees, with a narrow range of wind speeds around 5 m/s. Wind scenario 2 shows a broader distribution of wind coming from two main directions, around 225 and 270 degrees, with wind speeds varying from around 5 to over 13 m/s. Wind scenario 3 illustrates wind coming from multiple directions, predominantly from 90 and 135 degrees, with variable wind speeds, mostly between 5 and 9 m/s. Wind scenario 4 depicts a very varied wind profile with many directions involved, mainly from 135, 180, and 225 degrees, with wind speeds ranging widely from 4 to 15 m/s. The color scale on the right indicates wind speed in meters per second, with darker tones representing higher speeds. Each "petal" of the wind rose represents the frequency of the wind coming from that direction at that speed, with longer petals indicating a higher frequency of winds from that direction at the specified speed. Five state-of-the-art algorithms are used as performance comparison, including a comprehensive learning particle swarm optimizer (CLPSO) [75], AGA [25], SUGGA [26], a gravitational search algorithm with hierarchy and distributed framework (HGSA) [76], and the invasive weed optimization (IWO) [77]. For a pair comparison, the population size and maximum iteration number of all algorithms are set to 120 and 200, respectively. The detailed parameters are shown in Table 1. Other parameters of other algorithms are set according to its paper.

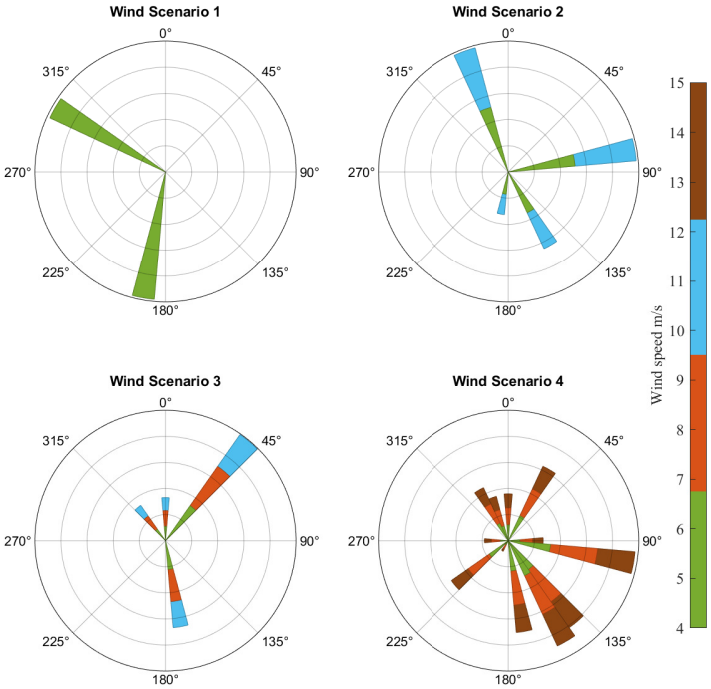

Figure 2. The wind rose illustrations for wind scenarios 1–4.

Table 1. The parameter setup of the algorithms.

Algorithm	Parameters
ACDE	$sf = 0.5, cr = 0.5, m_s = 5, c = 0.1, p = 0.05$
AGA	$p_e = 0.2, p_c = 0.6, p_m = 0.1, p_r = 0.5$
SUGGA	$p_e = 0.2, p_c = 0.6, p_m = 0.1, p_r = 0.5$
CLPSO	$c_1 = c_2 = 1.496, gap_m = 7$
IWO	$s_{min} = 2, s_{max} = 5, \delta_{init} = 0.5, \delta_{final} = 0.001$
HGSA	$G_0 = 100, L = 100, w_1(t) = 1 - t^6/T^6, w_2(t) = t^6/T^6$

Table 2. The experimental results of all algorithms.

Turbine		AGA	SUGGA	CLPSO	HGSA	IWO	ACDE
Wind scenario 1							
Average	15	99.35(0.24)	99.54(0.20)	97.97(0.38)	97.93(0.45)	98.67(0.33)	**99.66(0.18)**
	20	97.07(0.36)	97.49(0.36)	94.43(0.45)	94.56(0.56)	95.42(0.41)	**97.71(0.34)**
	30	94.49(0.37)	94.99(0.40)	91.16(0.51)	91.08(0.60)	91.98(0.48)	**95.25(0.37)**
	p-value	2.73E-08	4.70E-04	2.73E-04	2.73E-04	2.73E-04	–
Wind scenario 2							
Average	15	97.97(0.28)	98.16(0.27)	96.39(0.37)	96.88(0.38)	96.17(0.36)	**98.30(0.24)**
	20	95.49(0.35)	95.54(0.34)	92.98(0.37)	93.76(0.39)	93.01(0.33)	**96.03(0.29)**
	30	92.77(0.35)	92.74(0.36)	89.80(0.38)	90.68(0.38)	89.90(0.36)	**93.49(0.28)**
	p-value	2.73E-04	2.95E-04	2.73E-04	2.73E-04	2.73E-04	–
Wind scenario 3							
Average	15	98.01(0.24)	98.39(0.22)	96.58(0.36)	96.56(0.39)	97.11(0.30)	**98.48(0.22)**
	20	95.79(0.32)	96.40(0.37)	93.34(0.43)	93.03(0.49)	93.89(0.36)	**96.55(0.31)**
	30	93.37(0.38)	94.06(0.40)	90.07(0.57)	89.37(0.58)	90.42(0.46)	**94.21(0.36)**
	p-value	2.73E-04	5.09E-04	2.73E-04	2.73E-04	2.73E-04	–
Wind scenario 4							
Average	15	95.82(0.24)	95.75(0.26)	94.43(0.33)	94.79(0.27)	94.24(0.23)	**96.05(0.23)**
	20	92.85(0.27)	92.76(0.28)	91.02(0.31)	91.28(0.27)	90.99(0.23)	**93.24(0.23)**
	30	89.93(0.25)	89.85(0.29)	87.72(0.29)	87.98(0.29)	87.80(0.23)	**90.33(0.19)**
	p-value	2.63E-04	3.19E-04	2.73E-04	2.73E-04	2.73E-04	–

Table 2 summarizes all of the results under different wind scenarios and wind turbine numbers. It reports the average results of various constraints and the Wilcoxon test. The optimal results in each category are also emphasized in bold. The detailed experimental results are shown in the Supplementary File. Table S.I presents the experimental outcomes for various algorithms applied to wind scenario 1. The results for each algorithm are organized into rows labeled L0 to L12, which are further grouped into three categories based on turbine counts: 15, 20, and 25. The performance of the algorithms is evaluated against a spectrum of constraints, marked from L0 to L12, where L0 represents an unconstrained scenario. The constraints are illustrated in Figure 3. Each table entry includes two numbers: the energy conversion efficiency and its corresponding standard deviation. This table aggregates the average efficiencies for each turbine group and algorithm, along with the p-values from the Wilcoxon signed-rank test, to ascertain statistical significance. The table demonstrates that the proposed ACDE algorithm surpasses its counterparts in 38 out of 39 cases, except for the scenario with 25 turbines under the L12 constraint. Moreover, the Wilcoxon signed-rank test, uniformly applied across all experiments

with a significance level of 0.05, confirms that the ACDE algorithm significantly outperforms the rival algorithms in wind scenario 1.

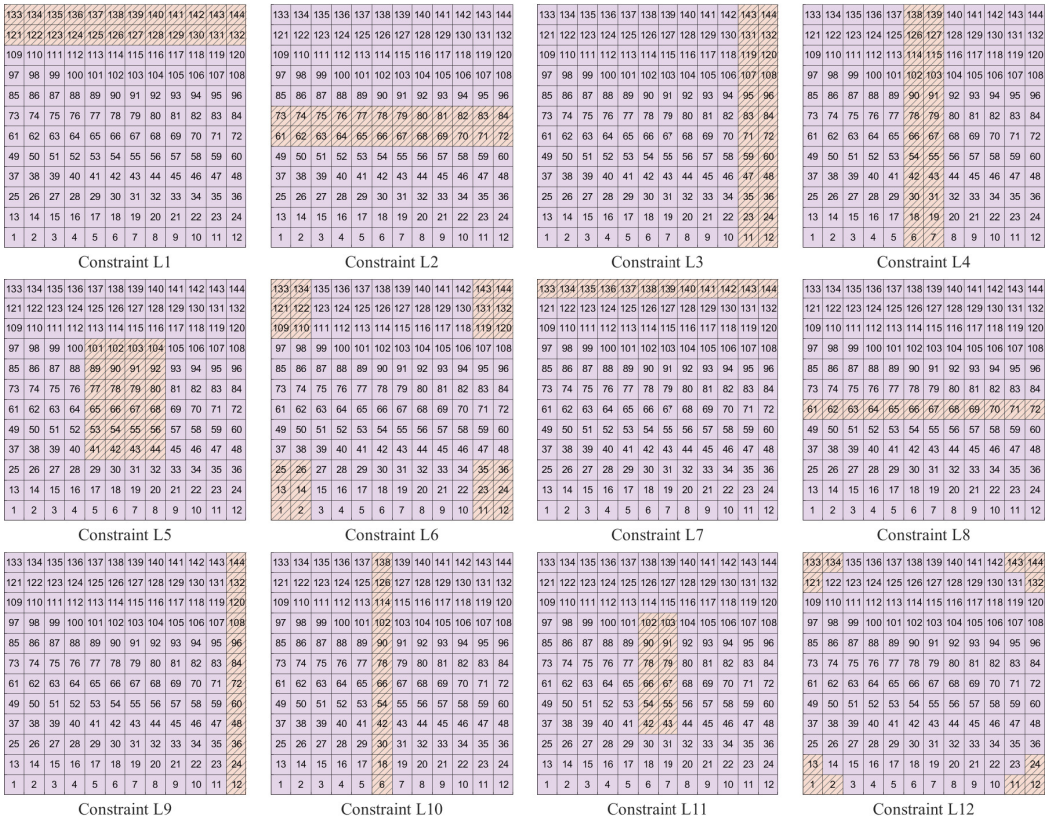

Figure 3. The illustration of the constraints.

Table S.II shows the experimental results of different algorithms on wind scenario 2. For instance, with 15 turbines, the ACDE algorithm shows the highest average efficiency at 98.30% (±0.24). This pattern of ACDE outperforming the other algorithms continues across the 20 and 25 turbine scenarios with average efficiencies of 96.03% (±0.29) and 93.49% (±0.28), respectively. The table also includes the p-values from the Wilcoxon signed-rank test, which are identical across all algorithms and scenarios (1.22E-04), suggesting a high level of statistical significance for the differences observed. In summary, Table S.II indicates that the ACDE algorithm consistently achieves higher efficiency compared to the other algorithms across all levels of constraints and turbine counts in wind scenario 2.

Table S.III details the experimental results of different algorithms on wind scenario 3. It is formatted similarly to the previous table and includes results for turbine counts of 15, 20, and 25. The best results within each constraint level are highlighted in bold. The ACDE algorithm consistently shows superior performance in most cases, with the highest average efficiencies for 15 turbines (98.48% ± 0.22), 20 turbines (96.55% ± 0.31), and 25 turbines (94.21% ± 0.36). The table also presents p-values from the Wilcoxon signed-rank test for each turbine group, indicating the statistical significance of the results. The p-values for 15 and 20 turbines are consistent across all algorithms (1.22E-04), implying highly significant results. The proposed ACDE algorithm surpasses its counterparts in 31 out of 39 cases on wind scenario 3. However, for the 25 turbine group, the p-value for the ACDE algorithm is notably different (2.87E-02), which is still below the threshold of 0.05 for statistical significance, suggesting

that the differences in performance are statistically significant. Overall, Table 3 demonstrates that the ACDE algorithm outperforms the other algorithms in wind scenario 3 across various levels of constraints and turbine counts.

Table S.IV shows the experimental results of various algorithms tested in wind scenario 4. The best results are highlighted in bold, indicating the highest efficiency achieved for each row. For the 15 turbine group, the ACDE algorithm shows the highest average efficiency (96.05% ± 0.23). In the 20 turbine group, ACDE again has the highest average efficiency (93.24% ± 0.23). For the 25 turbine group, ACDE maintains the lead with an average efficiency of 90.33% ± 0.19. All algorithms share the same p-values from the Wilcoxon signed-rank test for each turbine group (1.22E-04), suggesting strong statistical significance in the performance differences. In summary, Table S.IV demonstrates that the ACDE algorithm consistently outperforms the other algorithms in wind scenario 4, across all levels of constraints and turbine counts, with statistical significance.

Figure 4 gives the convergence plots to observe the search dynamics. The convergence plots of other wind scenarios are given in the Supplementary File. These figures contain three line graphs that constitute a convergence plot, comparing the performance of six algorithms—SUGGA, AGA, CLPSO, HGSA, IWO, and ACDE—across three different numbers of wind turbines: 15, 20, and 25. Each graph represents the convergence trend of the algorithms over a specified number of iterations, which are indicated on the x-axis, ranging from 0 to 200. The y-axis represents the conversion efficiency, with scales adjusted to fit the performance range for each turbine scenario. Figure 4 is illuminating to express the search dynamics. In the 15 turbine graph, all algorithms show a rapid increase in efficiency, reaching near or above 0.995 efficiency, with ACDE appearing to converge the fastest and reaching the highest efficiency. For 20 turbines, the convergence lines spread out more, with efficiencies ranging from around 0.94 to just below 0.98. ACDE again shows a quick convergence to the highest efficiency level. The 25 turbine graph displays the greatest diversity in performance, with efficiencies starting from just below 0.91 and reaching up to approximately 0.96. ACDE continues to demonstrate a rapid convergence, though with a slightly lower efficiency compared to the 15 and 20 turbine scenarios. Each algorithm's performance is marked by distinct symbols and line styles for easy identification. The trend lines indicate that while all algorithms improve their conversion efficiency as the number of function evaluations increases, ACDE consistently leads in convergence speed and efficiency across all three turbine counts. It is worth noting that the convergence trajectory of ACDE exhibits a distinctive ladder pattern, indicating its ability to effectively balance exploration and exploitation. When ACDE is trapped in local optima, the wind turbine adjustment strategy can enhance population diversity, facilitating exploration of promising regions. In contrast, other algorithms typically demonstrate inferior exploration capabilities compared to ACDE. Consequently, ACDE is better equipped to provide superior solutions.

To give more insights into the obtained results, Figure 5 illustrates the solution distributions. The box-and-whisker plots of other wind scenarios are given in the Supplementary File. The figure is a set of box-and-whisker plots illustrating the conversion efficiency of various algorithms across three different wind turbine scenarios: 15 turbines, 20 turbines, and 25 turbines. For each algorithm, the box represents the interquartile range (IQR), which contains the middle 50% of the data. The horizontal line inside the box marks the median of the data. The whiskers extend from the box to the highest and lowest values, excluding outliers. Outliers are marked with red plus signs and lie outside the range of the whiskers. The 15 turbine plot shows relatively tight clustering for all of the algo-

rithms, with medians around 0.99, indicating high efficiency. The ACDE algorithm shows a higher median efficiency and a smaller IQR, suggesting more consistent performance. In the 20 turbine plot, the medians slightly decrease as expected with increased complexity, but ACDE maintains a higher median compared to other algorithms and shows fewer outliers. For the 25 turbine plot, the efficiency medians drop further, reflecting the increased challenge with more turbines. The ACDE demonstrates not only the highest median efficiency but also greater variance, as evidenced by the longer whiskers and presence of outliers. Overall, the ACDE algorithm appears to exhibit superior and more consistent conversion efficiency across all scenarios. Particularly, in the 25 turbine scenario, it shows the most variability among all of the algorithms, which implies that ACDE has the ability of addressing complex problems.

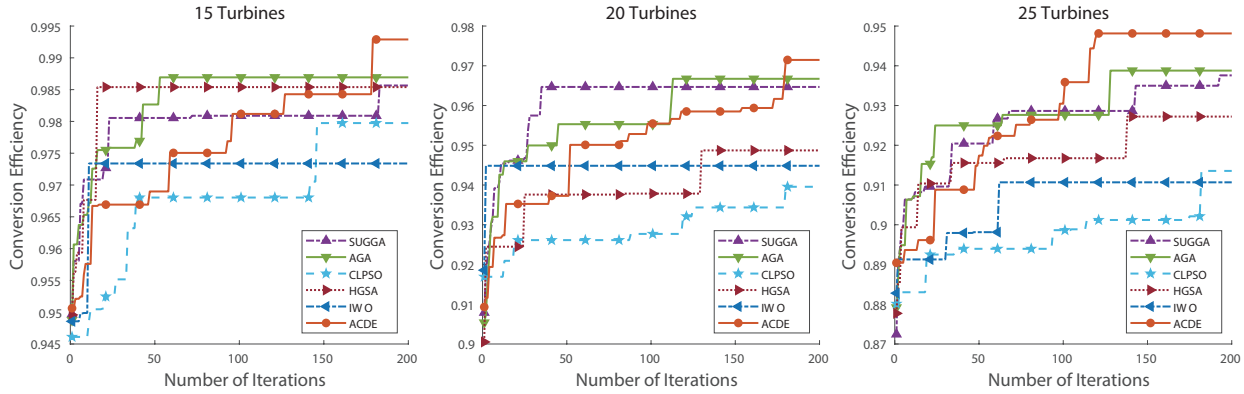

Figure 4. The convergence plot on wind scenario 2.

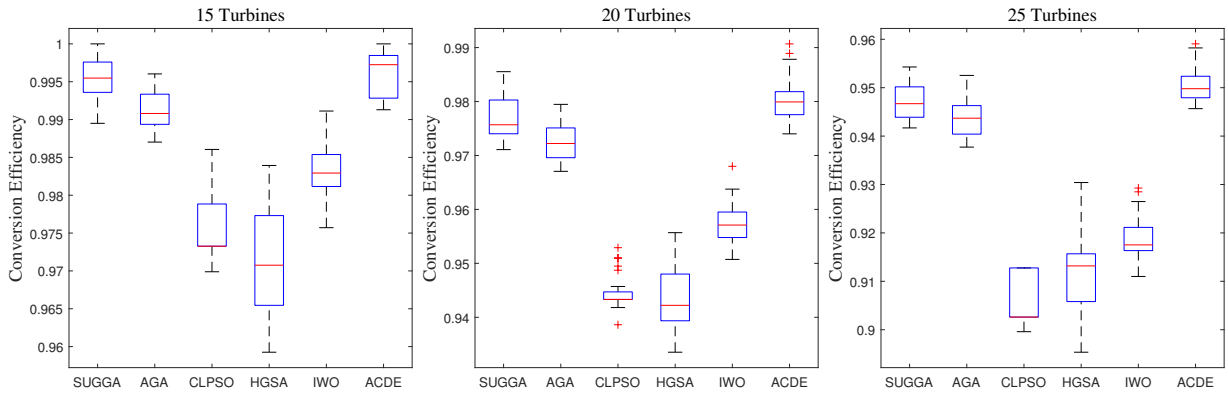

Figure 5. The box-and-whisker plot on wind scenario 1.

Additionally, Figures S.VII–S.IX give final wind farm layouts. The figure presents six grid layouts representing wind farm configurations under wind scenario 1 to 4, respectively, for all compared algorithms. Each grid layout is composed of numbered squares that represent individual turbine positions within the wind farm. The squares are color-coded with different symbols to possibly indicate the efficiency or another specific characteristic related to each turbine's placement. The configurations are unique for each algorithm, suggesting that each algorithm optimizes the wind farm layout differently. Beneath each grid layout, the efficiency value (η) is provided, which corresponds to the overall efficiency of the wind farm layout as determined by the respective algorithm. These values suggest

that the ACDE algorithm achieves the highest overall efficiency for the wind farm layout in all wind scenarios.

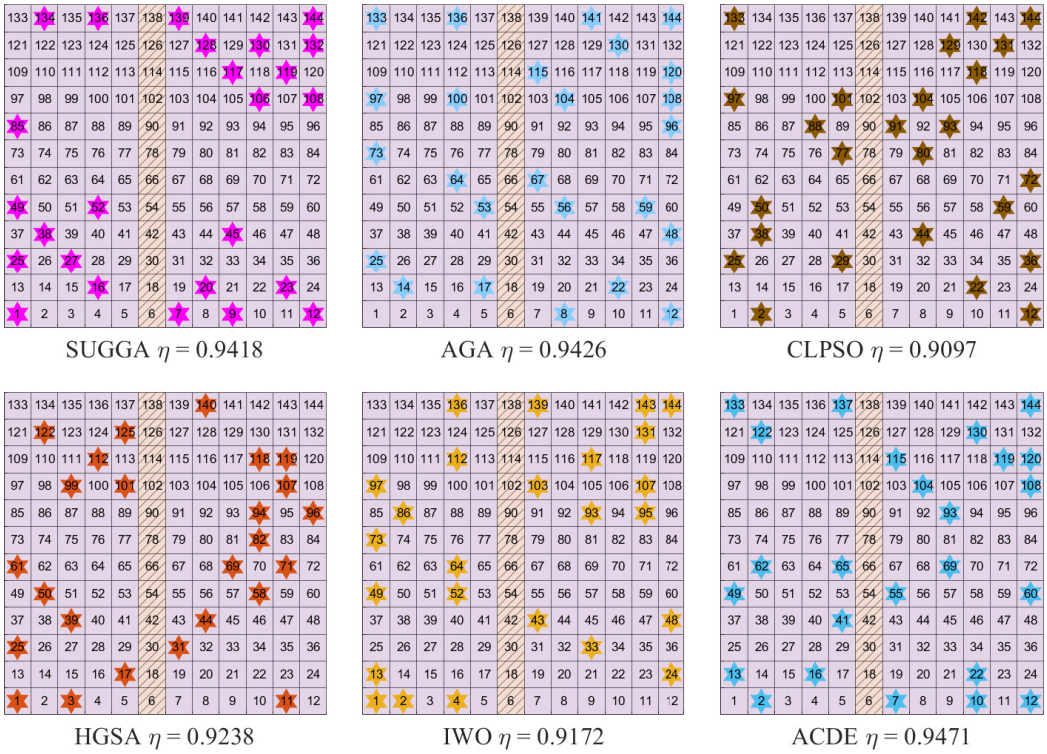

Figure 6. The wind farm layout plot under wind scenario 2.

More discussions are given regarding the parameter sensitivity and ablation study. First, Table 3 discusses the effect of *rad* ($\in \{0.01, 0.05, 0.1, 0.5\}$) in Eq (3.2), which is a hyper-parameter to control the scale of the chaotic local search. Table 3 shows the results of a parameter sensitivity analysis for different wind turbine scenarios, labeled WS1 (wind scenario 1) through WS4 (wind scenario 4). The table is divided into multiple columns, each representing a different set of parameter values (*rad* = 0.01, *rad* = 0.03, etc.). Within each parameter setting, there are multiple sub-columns for each of the wind scenarios (WS1–WS4), with each wind scenario further broken down into results for various constraint levels, labeled from L1 to L12. At the bottom of the table, the row "Total" sums up the overall performance or count for each set of parameters across all wind scenarios, which indicates that when *rad* is set to 0.5, ACDE has better performance than the others. To further assess the effect of the proposed novel power generation accumulation-based tournament selection method, an ablation study is performed. Table 4 lists the impact of selection on an adaptive replacement strategy. ACDE-R means a variant of using random selection. From this table, it is clearly observed that the tournament selection is significantly better than it.

The genetic and evolutionary computation conference (GECCO) hosts a wind farm layout optimization competition [78], featuring five intricate wind scenarios. The competition imposes a limit of 10,000 evaluations for all five scenarios. It is important to note that AGA and SUGGA are deemed unsuitable for this competition, as they are optimized for different modeling patterns. Consequently, they have been excluded from this comparison. In their place, a binary GA has been adopted, as recommended by the GECCO competition, to evaluate the performance of the algorithms. The objective

function for competitors is to minimize the cost of energy.

$$f = \frac{(c_t n + c_s \left\lfloor \frac{n}{m} \right\rfloor) + c_{OM} n}{(1 - (1 - r)^{-y})} * \frac{1}{8760P} + \frac{0.1}{n} \tag{4.1}$$

where c_t is the turbine cost, and c_s is the price of a substation. m and n are the number of turbines per substation and the layout r and y are the interest rate and the farm lifetime, respectively. c_{OM} is the operation and maintenance costs, and P is the power generation.

Table 3. The experimental results of the parameter discussion.

Parameter		*rad* = 0.01	*rad* = 0.05	*rad* = 0.1	*rad* = 0.5	*rad* = 0.01	*rad* = 0.05	*rad* = 0.1	*rad* = 0.5	*rad* = 0.01	*rad* = 0.05	*rad* = 0.1	*rad* = 0.5
Turbine		15				20				25			
	L0	**99.76(0.17)**	99.69(0.18)	99.69(0.17)	99.71(0.17)	97.79(0.26)	97.86(0.37)	97.81(0.35)	**97.91(0.35)**	95.58(0.39)	**95.59(0.39)**	95.55(0.44)	95.54(0.34)
	L1	99.67(0.16)	99.69(0.17)	99.65(0.23)	**99.70(0.19)**	97.49(0.40)	**97.50(0.34)**	97.47(0.40)	97.49(0.43)	94.71(0.40)	94.71(0.36)	**94.74(0.41)**	94.58(0.37)
	L2	99.80(0.12)	99.79(0.15)	**99.80(0.12)**	99.78(0.16)	98.14(0.28)	98.17(0.34)	98.16(0.34)	**98.22(0.29)**	96.03(0.33)	95.97(0.29)	**96.09(0.28)**	96.08(0.34)
	L3	99.21(0.20)	99.31(0.24)	**99.35(0.24)**	99.33(0.26)	**97.08(0.32)**	97.01(0.43)	97.07(0.36)	96.99(0.34)	94.43(0.46)	94.39(0.37)	**94.44(0.42)**	94.34(0.35)
	L4	99.77(0.21)	**99.80(0.15)**	99.79(0.16)	99.73(0.18)	97.87(0.31)	97.90(0.34)	97.91(0.35)	**97.95(0.34)**	**95.50(0.33)**	95.40(0.41)	95.47(0.39)	95.39(0.37)
	L5	99.72(0.14)	**99.72(0.16)**	99.70(0.15)	99.69(0.15)	98.01(0.27)	98.01(0.24)	98.01(0.32)	**98.03(0.23)**	95.83(0.29)	95.92(0.29)	95.90(0.31)	**95.99(0.36)**
WS1	L6	99.51(0.29)	99.51(0.23)	99.56(0.22)	**99.60(0.27)**	**97.32(0.32)**	97.19(0.34)	97.23(0.37)	97.25(0.37)	94.60(0.43)	94.45(0.38)	94.61(0.40)	**94.62(0.43)**
	L7	99.60(0.19)	**99.69(0.18)**	99.67(0.18)	99.68(0.19)	**97.74(0.36)**	97.68(0.35)	97.72(0.46)	97.67(0.36)	95.08(0.36)	95.03(0.39)	**95.08(0.39)**	95.07(0.35)
	L8	99.79(0.14)	99.77(0.18)	99.77(0.19)	**99.80(0.15)**	98.07(0.35)	**98.10(0.30)**	97.96(0.36)	98.04(0.33)	95.77(0.35)	**95.91(0.36)**	95.80(0.40)	95.85(0.41)
	L9	99.59(0.20)	**99.60(0.21)**	99.58(0.22)	99.55(0.18)	97.50(0.25)	**97.60(0.36)**	97.58(0.38)	97.51(0.30)	94.99(0.42)	95.08(0.36)	95.05(0.36)	**95.10(0.48)**
	L10	**99.73(0.19)**	99.71(0.18)	99.72(0.19)	99.71(0.15)	97.90(0.37)	**98.03(0.47)**	97.86(0.31)	97.94(0.41)	95.65(0.42)	95.56(0.40)	**95.66(0.39)**	95.52(0.34)
	L11	99.70(0.18)	99.74(0.15)	99.73(0.14)	**99.75(0.16)**	97.93(0.29)	**98.02(0.32)**	97.90(0.36)	97.94(0.24)	95.66(0.43)	**95.77(0.32)**	95.73(0.32)	95.75(0.41)
	L12	99.56(0.19)	99.53(0.20)	99.54(0.20)	**99.58(0.19)**	97.23(0.38)	97.29(0.33)	97.32(0.42)	**97.34(0.38)**	94.39(0.35)	94.49(0.47)	**94.56(0.40)**	94.43(0.33)
p-value		2.71E-01	3.18E-01	3.18E-01	–	1.88E-01	7.06E-01	1.08E-01	–	5.00E-01	6.32E-01	8.63E-01	–
	L0	98.45(0.29)	**98.46(0.28)**	98.45(0.26)	98.41(0.23)	96.26(0.28)	96.22(0.23)	96.23(0.30)	**96.31(0.29)**	**93.95(0.32)**	93.94(0.30)	93.85(0.25)	93.84(0.27)
	L1	98.02(0.25)	98.09(0.29)	98.07(0.28)	**98.10(0.30)**	95.55(0.35)	95.57(0.28)	95.60(0.31)	**95.61(0.24)**	**92.90(0.33)**	92.81(0.26)	92.86(0.28)	92.80(0.30)
	L2	98.46(0.21)	98.50(0.22)	**98.52(0.21)**	98.50(0.24)	96.41(0.21)	96.38(0.22)	96.40(0.26)	**96.51(0.33)**	94.01(0.23)	93.89(0.23)	94.00(0.29)	**94.02(0.28)**
	L3	**98.07(0.28)**	98.02(0.33)	98.04(0.24)	98.02(0.26)	**95.58(0.32)**	95.51(0.31)	95.55(0.31)	95.50(0.35)	92.71(0.25)	**92.74(0.29)**	92.70(0.29)	92.72(0.29)
	L4	98.56(0.21)	98.52(0.24)	**98.58(0.22)**	98.55(0.21)	96.51(0.22)	96.52(0.26)	**96.53(0.29)**	96.50(0.28)	94.04(0.32)	94.10(0.26)	**94.12(0.27)**	94.07(0.32)
	L5	98.47(0.19)	98.47(0.19)	98.46(0.21)	**98.48(0.24)**	96.44(0.26)	96.37(0.27)	**96.47(0.30)**	96.37(0.33)	**94.11(0.28)**	94.07(0.26)	94.09(0.22)	94.09(0.25)
WS2	L6	97.77(0.26)	97.69(0.25)	97.74(0.26)	**97.78(0.30)**	95.16(0.26)	95.15(0.25)	95.15(0.33)	**95.21(0.30)**	92.39(0.32)	**92.49(0.37)**	92.41(0.30)	92.43(0.29)
	L7	98.25(0.22)	**98.30(0.31)**	98.28(0.27)	98.26(0.25)	95.92(0.23)	**95.96(0.31)**	95.93(0.28)	95.90(0.26)	93.30(0.26)	93.31(0.30)	93.35(0.22)	**93.37(0.32)**
	L8	98.49(0.24)	98.48(0.21)	98.48(0.22)	**98.52(0.21)**	96.41(0.28)	**96.43(0.29)**	96.34(0.25)	96.33(0.24)	93.94(0.28)	93.96(0.30)	93.95(0.32)	**94.00(0.29)**
	L9	98.20(0.28)	98.24(0.20)	**98.28(0.23)**	98.24(0.20)	**95.95(0.32)**	95.88(0.29)	95.92(0.34)	95.86(0.28)	93.31(0.27)	**93.35(0.35)**	93.35(0.28)	93.30(0.24)
	L10	**98.48(0.21)**	98.41(0.26)	98.43(0.28)	98.45(0.18)	**96.36(0.29)**	96.35(0.23)	96.31(0.25)	96.30(0.30)	**94.00(0.40)**	93.94(0.31)	93.98(0.33)	93.95(0.26)
	L11	98.47(0.25)	98.45(0.21)	**98.52(0.30)**	98.44(0.22)	96.32(0.26)	**96.44(0.29)**	96.36(0.30)	96.33(0.28)	93.93(0.26)	93.92(0.24)	93.93(0.25)	**93.96(0.30)**
	L12	98.11(0.30)	98.08(0.28)	98.05(0.26)	**98.11(0.30)**	95.57(0.32)	95.61(0.33)	**95.65(0.35)**	95.62(0.27)	92.82(0.34)	**92.92(0.34)**	92.82(0.29)	92.88(0.30)
p-value		3.42E-01	2.27E-01	5.80E-01	–	7.29E-01	6.32E-01	7.73E-01	–	3.68E-01	6.07E-01	4.20E-01	–
	L0	98.62(0.22)	98.65(0.20)	**98.67(0.24)**	98.66(0.23)	96.77(0.31)	96.94(0.36)	96.71(0.32)	**96.97(0.38)**	94.69(0.49)	94.67(0.42)	**94.70(0.36)**	94.55(0.38)
	L1	**98.19(0.22)**	98.14(0.24)	98.17(0.25)	98.17(0.21)	96.01(0.31)	96.02(0.32)	96.07(0.31)	**96.07(0.35)**	93.58(0.34)	93.60(0.38)	93.56(0.28)	**93.65(0.33)**
	L2	99.01(0.15)	98.94(0.17)	98.96(0.17)	**99.01(0.18)**	97.39(0.28)	97.46(0.29)	97.35(0.25)	**97.47(0.24)**	**95.41(0.43)**	95.37(0.34)	95.29(0.25)	95.21(0.27)
	L3	98.22(0.26)	**98.30(0.26)**	98.22(0.27)	98.22(0.30)	96.00(0.35)	95.97(0.36)	**96.06(0.32)**	95.98(0.45)	93.37(0.39)	93.37(0.43)	93.39(0.52)	**93.42(0.41)**
	L4	98.23(0.19)	**98.26(0.21)**	98.19(0.23)	98.20(0.20)	**96.17(0.30)**	96.02(0.24)	96.10(0.28)	96.14(0.32)	**93.70(0.31)**	93.69(0.35)	93.67(0.37)	93.64(0.30)
	L5	98.99(0.14)	**99.00(0.14)**	98.97(0.14)	98.99(0.14)	97.47(0.28)	97.46(0.29)	**97.53(0.30)**	97.45(0.23)	**95.34(0.33)**	95.29(0.31)	95.23(0.31)	95.31(0.32)
WS3	L6	**98.05(0.25)**	98.04(0.23)	98.04(0.19)	98.02(0.23)	95.76(0.31)	**95.76(0.36)**	95.74(0.34)	95.66(0.28)	93.24(0.39)	93.27(0.30)	**93.28(0.40)**	93.24(0.31)
	L7	98.48(0.22)	**98.49(0.20)**	98.45(0.24)	98.37(0.24)	96.53(0.29)	96.55(0.34)	**96.58(0.39)**	96.42(0.34)	**94.28(0.42)**	94.14(0.32)	94.10(0.36)	94.17(0.36)
	L8	**98.82(0.22)**	98.80(0.24)	98.79(0.20)	98.78(0.20)	97.08(0.30)	97.08(0.36)	97.11(0.31)	**97.12(0.29)**	94.95(0.26)	95.00(0.44)	95.03(0.47)	**95.10(0.36)**
	L9	98.44(0.31)	98.46(0.24)	**98.47(0.20)**	98.46(0.24)	96.41(0.34)	96.46(0.43)	**96.48(0.37)**	96.48(0.34)	93.97(0.40)	94.10(0.46)	94.09(0.35)	**94.19(0.37)**
	L10	98.43(0.18)	98.46(0.23)	98.42(0.22)	**98.52(0.26)**	**96.58(0.32)**	96.52(0.39)	96.45(0.28)	96.53(0.26)	**94.31(0.42)**	94.24(0.31)	94.23(0.30)	94.27(0.45)
	L11	98.83(0.18)	**98.85(0.20)**	98.81(0.20)	98.80(0.19)	97.12(0.28)	97.13(0.29)	**97.27(0.32)**	97.10(0.31)	94.95(0.41)	**94.97(0.37)**	94.95(0.39)	94.96(0.38)
	L12	98.04(0.23)	98.05(0.22)	**98.12(0.27)**	98.06(0.24)	**95.74(0.35)**	95.69(0.26)	95.67(0.29)	95.71(0.30)	**93.03(0.33)**	92.98(0.28)	93.00(0.28)	93.01(0.43)
p-value		7.06E-01	8.30E-01	6.82E-01	–	5.00E-01	2.07E-01	6.32E-01	–	6.32E-01	3.42E-01	1.70E-01	–
	L0	**96.36(0.25)**	96.34(0.24)	96.35(0.17)	96.33(0.20)	**93.76(0.27)**	93.74(0.24)	93.70(0.23)	93.68(0.19)	90.92(0.19)	**90.97(0.23)**	90.91(0.21)	90.96(0.19)
	L1	95.54(0.20)	95.52(0.23)	**95.59(0.28)**	95.54(0.22)	92.48(0.22)	92.40(0.21)	**92.48(0.24)**	92.47(0.22)	89.36(0.16)	**89.41(0.21)**	89.40(0.17)	89.37(0.19)
	L2	**96.35(0.22)**	96.32(0.22)	96.32(0.19)	96.29(0.21)	93.56(0.20)	93.50(0.21)	93.53(0.19)	**93.59(0.25)**	90.69(0.17)	90.69(0.15)	90.66(0.19)	**90.72(0.20)**
	L3	95.53(0.22)	95.53(0.25)	**95.59(0.26)**	95.53(0.20)	92.46(0.24)	**92.55(0.29)**	92.46(0.21)	92.50(0.25)	89.39(0.19)	89.40(0.22)	**89.45(0.23)**	89.44(0.20)
	L4	96.24(0.18)	**96.30(0.20)**	96.27(0.23)	96.29(0.21)	93.53(0.17)	**93.62(0.21)**	93.60(0.21)	93.61(0.19)	90.83(0.20)	90.79(0.16)	90.85(0.19)	**90.88(0.16)**
	L5	96.41(0.19)	96.37(0.19)	96.34(0.21)	**96.42(0.30)**	93.66(0.21)	93.67(0.21)	93.72(0.18)	**93.74(0.23)**	90.97(0.18)	90.98(0.22)	**91.00(0.21)**	91.00(0.20)
WS4	L6	95.48(0.24)	**95.50(0.26)**	95.46(0.21)	95.44(0.22)	**92.19(0.21)**	92.17(0.20)	92.16(0.25)	92.15(0.20)	88.87(0.23)	**88.88(0.19)**	88.87(0.21)	88.86(0.23)
	L7	**95.97(0.27)**	95.95(0.20)	95.97(0.19)	95.97(0.22)	93.14(0.23)	93.16(0.28)	93.14(0.23)	**93.22(0.29)**	**90.26(0.23)**	90.26(0.22)	90.22(0.21)	90.23(0.19)
	L8	96.33(0.20)	**96.38(0.25)**	96.34(0.26)	96.32(0.26)	93.66(0.25)	93.63(0.21)	**93.73(0.23)**	93.64(0.21)	90.92(0.23)	90.93(0.22)	90.88(0.21)	**90.94(0.17)**
	L9	95.97(0.23)	95.96(0.25)	**96.05(0.21)**	95.93(0.22)	93.13(0.22)	**93.16(0.22)**	93.06(0.20)	93.07(0.26)	**90.22(0.20)**	90.21(0.20)	90.19(0.21)	90.20(0.20)
	L10	96.37(0.25)	96.37(0.24)	**96.41(0.21)**	96.35(0.24)	93.68(0.23)	93.68(0.22)	93.70(0.23)	**93.75(0.27)**	90.94(0.25)	90.95(0.19)	90.89(0.19)	**90.98(0.19)**
	L11	96.36(0.18)	**96.38(0.23)**	96.38(0.21)	96.34(0.22)	93.70(0.23)	93.64(0.19)	93.71(0.25)	**93.76(0.20)**	90.96(0.23)	90.92(0.19)	**91.00(0.23)**	90.96(0.19)
	L12	**95.94(0.20)**	95.89(0.27)	95.87(0.22)	95.85(0.22)	92.86(0.21)	92.84(0.22)	92.85(0.19)	**92.90(0.23)**	**89.81(0.23)**	89.79(0.23)	89.80(0.24)	89.77(0.22)
Total		11	**15**	13	13	11	12	10	**19**	14	11	12	**15**

Table 4. The experimental results of the ablation study.

Selection Method		ACDE-R	ACDE	ACDE-R	ACDE	ACDE-R	ACDE
Turbine		15		20		25	
	L0	99.55(0.20)	**99.71(0.17)**	97.56(0.32)	**97.91(0.35)**	95.01(0.33)	**95.54(0.34)**
	L1	99.20(0.33)	**99.70(0.19)**	96.66(0.38)	**97.49(0.43)**	94.06(0.57)	**94.58(0.37)**
	L2	99.30(0.27)	**99.78(0.16)**	97.39(0.33)	**98.22(0.29)**	95.22(0.41)	**96.08(0.34)**
	L3	98.64(0.32)	**99.33(0.26)**	96.12(0.39)	**96.99(0.34)**	93.50(0.38)	**94.34(0.35)**
	L4	99.24(0.31)	**99.73(0.18)**	97.10(0.41)	**97.95(0.34)**	94.57(0.41)	**95.39(0.37)**
	L5	99.32(0.30)	**99.69(0.15)**	97.34(0.32)	**98.03(0.23)**	95.12(0.35)	**95.99(0.36)**
WS1	L6	99.01(0.32)	**99.60(0.27)**	96.55(0.48)	**97.25(0.37)**	93.85(0.41)	**94.62(0.43)**
	L7	99.41(0.38)	**99.68(0.19)**	97.16(0.45)	**97.67(0.36)**	94.46(0.46)	**95.07(0.35)**
	L8	99.36(0.19)	**99.80(0.15)**	97.50(0.40)	**98.04(0.33)**	95.06(0.34)	**95.85(0.41)**
	L9	99.10(0.38)	**99.55(0.18)**	96.97(0.47)	**97.51(0.30)**	94.34(0.28)	**95.10(0.48)**
	L10	99.43(0.24)	**99.71(0.15)**	97.25(0.40)	**97.94(0.41)**	94.83(0.39)	**95.52(0.34)**
	L11	99.38(0.24)	**99.75(0.16)**	97.36(0.30)	**97.94(0.24)**	95.09(0.39)	**95.75(0.41)**
	L12	99.09(0.38)	**99.58(0.19)**	96.68(0.44)	**97.34(0.38)**	93.97(0.38)	**94.43(0.33)**
p-value		1.22E-04	–	1.22E-04	–	1.22E-04	–
	L0	98.18(0.26)	**98.41(0.23)**	95.91(0.26)	**96.31(0.29)**	93.58(0.28)	**93.84(0.27)**
	L1	97.60(0.36)	**98.10(0.30)**	94.96(0.31)	**95.61(0.24)**	92.38(0.34)	**92.80(0.30)**
	L2	97.90(0.35)	**98.50(0.24)**	95.82(0.34)	**96.51(0.33)**	93.49(0.29)	**94.02(0.28)**
	L3	97.43(0.32)	**98.02(0.26)**	94.99(0.39)	**95.50(0.35)**	92.19(0.35)	**92.72(0.29)**
	L4	97.98(0.24)	**98.55(0.21)**	95.89(0.30)	**96.50(0.28)**	93.57(0.30)	**94.07(0.32)**
	L5	97.98(0.25)	**98.48(0.24)**	95.89(0.31)	**96.37(0.33)**	93.59(0.32)	**94.09(0.25)**
WS2	L6	97.20(0.31)	**97.78(0.30)**	94.68(0.37)	**95.21(0.30)**	92.01(0.37)	**92.43(0.29)**
	L7	97.83(0.38)	**98.26(0.25)**	95.49(0.29)	**95.90(0.26)**	92.94(0.26)	**93.37(0.32)**
	L8	98.13(0.27)	**98.52(0.21)**	96.00(0.36)	**96.33(0.24)**	93.61(0.33)	**94.00(0.29)**
	L9	97.85(0.24)	**98.24(0.20)**	95.42(0.25)	**95.86(0.28)**	92.86(0.26)	**93.30(0.24)**
	L10	98.12(0.27)	**98.45(0.18)**	95.82(0.36)	**96.30(0.30)**	93.53(0.25)	**93.95(0.26)**
	L11	98.05(0.24)	**98.44(0.22)**	95.93(0.34)	**96.33(0.28)**	93.47(0.31)	**93.96(0.30)**
	L12	97.60(0.31)	**98.11(0.30)**	95.19(0.40)	**95.62(0.27)**	92.48(0.35)	**92.88(0.30)**
p-value		1.22E-04	–	1.22E-04	–	1.22E-04	–
	L0	98.63(0.24)	**98.66(0.23)**	96.61(0.30)	**96.97(0.38)**	94.26(0.32)	**94.55(0.38)**
	L1	97.91(0.28)	**98.17(0.21)**	95.69(0.34)	**96.07(0.35)**	92.92(0.31)	**93.65(0.33)**
	L2	98.54(0.20)	**99.01(0.18)**	96.74(0.27)	**97.47(0.24)**	94.44(0.27)	**95.21(0.27)**
	L3	97.76(0.27)	**98.22(0.30)**	95.18(0.36)	**95.98(0.45)**	92.44(0.42)	**93.42(0.41)**
	L4	97.91(0.24)	**98.20(0.20)**	95.60(0.23)	**96.14(0.32)**	93.01(0.34)	**93.64(0.30)**
	L5	98.58(0.19)	**98.99(0.14)**	96.85(0.39)	**97.45(0.23)**	94.44(0.40)	**95.31(0.32)**
WS3	L6	97.84(0.31)	**98.02(0.23)**	95.41(0.28)	**95.66(0.28)**	92.76(0.36)	**93.24(0.31)**
	L7	98.20(0.22)	**98.37(0.24)**	96.13(0.20)	**96.42(0.34)**	93.67(0.39)	**94.17(0.36)**
	L8	98.50(0.18)	**98.78(0.20)**	96.65(0.35)	**97.12(0.29)**	94.27(0.33)	**95.10(0.36)**
	L9	98.23(0.26)	**98.46(0.24)**	95.98(0.34)	**96.48(0.34)**	93.59(0.56)	**94.19(0.37)**
	L10	98.23(0.28)	**98.52(0.26)**	96.22(0.30)	**96.53(0.26)**	93.70(0.32)	**94.27(0.45)**
	L11	98.50(0.24)	**98.80(0.19)**	96.71(0.27)	**97.10(0.31)**	94.26(0.34)	**94.96(0.38)**
	L12	97.84(0.26)	**98.06(0.24)**	95.32(0.30)	**95.71(0.30)**	92.65(0.38)	**93.01(0.43)**
p-value		1.22E-04	–	1.22E-04	–	1.22E-04	–
	L0	96.20(0.18)	**96.33(0.20)**	93.52(0.24)	**93.68(0.19)**	90.81(0.20)	**90.96(0.19)**
	L1	95.13(0.26)	**95.54(0.22)**	92.11(0.22)	**92.47(0.22)**	89.14(0.20)	**89.37(0.19)**
	L2	95.90(0.26)	**96.29(0.21)**	93.19(0.23)	**93.59(0.25)**	90.43(0.18)	**90.72(0.20)**
	L3	95.18(0.29)	**95.53(0.20)**	92.12(0.25)	**92.50(0.25)**	89.15(0.22)	**89.44(0.20)**
	L4	95.95(0.22)	**96.29(0.21)**	93.30(0.30)	**93.61(0.19)**	90.60(0.19)	**90.88(0.16)**
	L5	95.94(0.20)	**96.42(0.30)**	93.41(0.21)	**93.74(0.23)**	90.70(0.17)	**91.00(0.20)**
WS4	L6	95.04(0.31)	**95.44(0.22)**	91.83(0.27)	**92.15(0.20)**	88.60(0.19)	**88.86(0.23)**
	L7	95.65(0.27)	**95.97(0.22)**	92.88(0.24)	**93.22(0.29)**	89.98(0.18)	**90.23(0.19)**
	L8	96.02(0.22)	**96.32(0.26)**	93.43(0.30)	**93.64(0.21)**	90.72(0.22)	**90.94(0.17)**
	L9	95.64(0.22)	**95.93(0.22)**	92.75(0.21)	**93.07(0.26)**	89.99(0.19)	**90.20(0.20)**
	L10	96.07(0.28)	**96.35(0.24)**	93.43(0.27)	**93.75(0.27)**	90.70(0.16)	**90.98(0.19)**
	L11	96.07(0.27)	**96.34(0.22)**	93.40(0.27)	**93.76(0.20)**	90.73(0.22)	**90.96(0.19)**
	L12	95.54(0.23)	**95.85(0.22)**	92.61(0.29)	**92.90(0.23)**	89.53(0.23)	**89.77(0.22)**
p-value		1.22E-04	–	1.22E-04	–	1.22E-04	–

The results presented in Table 5 highlight the formidable competitiveness of ACDE. It is evident that IWO, HGSA, and CLPSO outperform the binary GA recommended by the GECCO competition, underscoring their capability to address the competition's challenges. Notably, ACDE emerges as the top-performing algorithm across all five scenarios, demonstrating its adeptness in handling complex optimization problems. Additionally, we compared ACDE with the winning algorithms of the 2014 GECCO competition, as shown in Table 6. Due to the fixed number of wind turbines, ACDE achieved competitive results, outperforming the algorithms that placed 2nd, 3rd, and 4th in scenarios 1, 2, and 4. In scenarios 3 and 5, ACDE also produced competitive solutions, further validating the effectiveness of our proposed method. The experimental results from GECCO indicate that ACDE can effectively handle discrete optimization problems with a fixed number of wind turbines in WFO. However, for scenarios involving a dynamic number of wind turbines, ACDE is not suitable due to its encoding limitations. Specifically, ACDE uses integer encoding to construct the wind farm, which requires the number of wind turbines to remain fixed.

Table 5. Cost of energy, compared to the state-of-the-art layout optimizations.

Scenarios	GA	IWO	HGSA	CLPSO	ACDE
1	1.269E-3	1.244E-3	1.254E-3	1.247E-3	**1.241E-3**
2	1.158E-3	1.162E-4	1.136E-3	1.114E-3	**1.106E-3**
3	6.913E-4	6.743E-4	6.671E-4	6.768E-4	**6.678E-4**
4	7.186E-4	6.991E-4	6.966E-4	7.001E-4	**6.963E-4**
5	1.269E-3	1.245E-4	1.226E-3	1.248E-3	**1.224E-3**

Table 6. Wake free ratio, compared to the state-of-the-art layout optimizations.

Scenarios	Wagner	Loshchilov	CMA-ES	GA	ACDE
1	0.9157	0.9402	0.8996	0.9021	0.9191
2	0.9112	0.9305	0.9100	0.9051	0.9116
3	0.8535	0.8798	0.8453	0.8570	0.8516
4	0.8777	0.9076	0.8768	0.8775	0.8803
5	0.8373	0.8649	0.8269	0.8482	0.8327

5. Conclusions

In this study, we introduced an innovative adaptive chaotic differential evolution (ACDE) algorithm designed to optimize wind turbine placement. This algorithm was specifically engineered to balance local exploitation and global exploration effectively, while incorporating problem-specific knowledge into its search mechanism. The ACDE algorithm enhanced the traditional DE method by integrating an adaptive chaotic local search and a pioneering wind turbine adjustment strategy based on tournament selection. The latter was crafted to give precedence to energy-efficient turbine placements, enhancing population diversity and surpassing the limitations of conventional meta-heuristic algorithms. The chaotic search applied to the global best individual enhanced algorithmic exploitation, while the proposed wind turbine adjustment strategy improved population diversity, ensuring effective algorithmic exploration. To further validate algorithm performance, comprehensive datasets of complex wind farm

layouts from GECCO's competition were utilized. The results unequivocally affirm ACDE has the ability of addressing complex optimization problems. Specifically, it obtained competitive results with the 2014 GECCO competition. However, it is noteworthy that the integration of the chaotic search and adjustment strategy did entail a certain increase in computational costs. Meanwhile, the performance of ACDE was limited for dynamic wind farm layout optimization on GECCO second edition.

Our comprehensive evaluations of ACDE, set against a variety of wind rose patterns and layout constraints, revealed its superiority over five cutting-edge algorithms. Its effectiveness was consistently demonstrated through higher average conversion efficiencies and statistically significant results in all tested wind scenarios and turbine counts, supported by experimental data and Wilcoxon signed-rank tests with p-values well below the 0.05 threshold. Graphical analyses, including box-and-whisker plots and convergence graphs, affirmed ACDE's robustness and dependability. These analyses accentuated ACDE's compact interquartile ranges, elevated median efficiencies, and rapid convergence rates, underscoring its capacity to sustain consistent performance amidst increasing scenario complexity. Remarkably, in scenarios with a larger number of turbines, ACDE not only achieved the highest median efficiency but also displayed significant variance, showcasing its versatility and superior performance under intricate conditions. The algorithm's effectiveness was also evident in the detailed wind farm layouts, where ACDE consistently attained the highest overall efficiency. A sensitivity analysis of the *rad* parameter further strengthened this result, with ACDE performing optimally when *rad* was set to 0.5—this points to a well-calibrated balance between exploration and exploitation within the algorithm's operational dynamics. The ablation study conclusively illustrated the positive effects of the innovative power generation accumulation-based tournament selection method implemented within ACDE. When compared to a variant using a random selection approach, the tournament selection method clearly emerged as a substantial factor contributing to ACDE's enhanced performance. In sum, the results from the experimental assessments, graphical depictions, parameter sensitivity analysis, and ablation study collectively solidified ACDE as an exceptionally capable and trustworthy methodology for wind farm layout optimization. This marks a notable improvement over current strategies in the field of wind energy optimization. In future work, we plan to optimize the encoding method and operators of the proposed algorithm to better address various types of problems, including dynamic problems.

Use of AI tools declaration

The authors declare they have not used Artificial Intelligence (AI) tools in the creation of this article.

Acknowledgments

This research was partially supported by the project of Talent Development of Taizhou University (No. QD2016061) and the Natural Science Foundation of the Jiangsu Higher Education Institutions of China (No. 19KJB520057).

Conflict of interest

The authors declare there is no conflicts of interest.

References

1. B. Lin, Z. Li, Towards world's low carbon development: The role of clean energy, *Appl. Energy*, **307** (2022), 118160. https://doi.org/10.1016/j.apenergy.2021.118160
2. Z. Liu, X. He, Balancing-oriented hydropower operation makes the clean energy transition more affordable and simultaneously boosts water security, *Nat. Water*, **1** (2023), 778–789. https://doi.org/10.1038/s44221-023-00126-0
3. S. Carley, D. M. Konisky, The justice and equity implications of the clean energy transition, *Nat. Energy*, **5** (2020), 569–577. https://doi.org/10.1038/s41560-020-0641-6
4. Z. Yu, H. W. Kamran, A. Amin, B. Ahmed, S. Peng, Sustainable synergy via clean energy technologies and efficiency dynamics, *Renewable Sustainable Energy Rev.*, **187** (2023), 113744. https://doi.org/10.1016/j.rser.2023.113744
5. H. T. Pao, Y. Y. Li, H. C. Fu, Clean energy, non-clean energy, and economic growth in the mist countries, *Energy Policy*, **67** (2014), 932–942. https://doi.org/10.1016/j.enpol.2013.12.039
6. S. Farid, S. Karim, M. A. Naeem, R. Nepal, T. Jamasb, Co-movement between dirty and clean energy: A time-frequency perspective, *Energy Econ.*, **119** (2023), 106565. https://doi.org/10.1016/j.eneco.2023.106565
7. Y. Wang, Y. Yu, S. Cao, X. Zhang, S. Gao, A review of applications of artificial intelligent algorithms in wind farms, *Artif. Intell. Rev.*, **53** (2020), 3447–3500. https://doi.org/10.1007/s10462-019-09768-7
8. S. Roga, S. Bardhan, Y. Kumar, S. K. Dubey, Recent technology and challenges of wind energy generation: A review, *Sustainable Energy Technol. Assess.*, **52** (2022), 102239. https://doi.org/10.1016/j.seta.2022.102239
9. P. Sadorsky, Wind energy for sustainable development: Driving factors and future outlook, *J. Cleaner Prod.*, **289** (2021), 125779. https://doi.org/10.1016/j.jclepro.2020.125779
10. Y. F. Nassar, H. J. El-Khozondar, W. El-Osta, S. Mohammed, M. Elnaggar, M. Khaleel, et al., Carbon footprint and energy life cycle assessment of wind energy industry in libya, *Energy Convers. Manage.*, **300** (2024), 117846. https://doi.org/10.1016/j.enconman.2023.117846
11. G. Msigwa, J. O. Ighalo, P. S. Yap, Considerations on environmental, economic, and energy impacts of wind energy generation: Projections towards sustainability initiatives, *Sci. Total Environ.*, **849** (2022), 157755. https://doi.org/10.1016/j.scitotenv.2022.157755
12. M. S. Nazir, N. Ali, M. Bilal, H. M. Iqbal, Potential environmental impacts of wind energy development: A global perspective, *Curr. Opin. Environ. Sci. Health*, **13** (2020), 85–90. https://doi.org/10.1016/j.coesh.2020.01.002
13. C. Jung, D. Schindler, Efficiency and effectiveness of global onshore wind energy utilization, *Energy Convers. Manage.*, **280** (2023), 116788. https://doi.org/10.1016/j.enconman.2023.116788
14. M. Hannan, A. Q. Al-Shetwi, M. Mollik, P. J. Ker, M. Mannan, M. Mansor, et al., Wind energy conversions, controls, and applications: A review for sustainable technologies and directions, *Sustainability*, **15** (2023), 3986. https://doi.org/10.3390/su15053986

15. G. Gualtieri, Comparative analysis and improvement of grid-based wind farm layout optimization, *Energy Convers. Manage.*, **208** (2020), 112593. https://doi.org/10.1016/j.enconman.2020.112593

16. R. Nash, R. Nouri, A. Vasel-Be-Hagh, Wind turbine wake control strategies: A review and concept proposal, *Energy Convers. Manage.*, **245** (2021), 114581. https://doi.org/10.1016/j.enconman.2021.114581

17. S. R. Reddy, An efficient method for modeling terrain and complex terrain boundaries in constrained wind farm layout optimization, *Renewable Energy*, **165** (2021), 162–173. https://doi.org/10.1016/j.renene.2020.10.076

18. P. Mittal, K. Mitra, In search of flexible and robust wind farm layouts considering wind state uncertainty, *J. Cleaner Prod.*, **248** (2020), 119195. https://doi.org/10.1016/j.jclepro.2019.119195

19. H. Sun, H. Yang, Wind farm layout and hub height optimization with a novel wake model, *Appl. Energy*, **348** (2023), 121554. https://doi.org/10.1016/j.apenergy.2023.121554

20. F. P. Garcia Marquez, A. Peinado Gonzalo, A comprehensive review of artificial intelligence and wind energy, *Arch. Comput. Methods Eng.*, **29** (2022), 2935–2958. https://doi.org/10.1007/s11831-021-09678-4

21. Q. Sui, Y. Yu, K. Wang, L. Zhong, Z. Lei, S. Gao, Best-worst individuals driven multiple-layered differential evolution, *Inf. Sci.*, **655** (2024), 119889. https://doi.org/10.1016/j.ins.2023.119889

22. S. Gao, Y. Yu, Y. Wang, J. Wang, J. Cheng, M. Zhou, Chaotic local search-based differential evolution algorithms for optimization, *IEEE Trans. Syst. Man Cybern.: Syst.*, **51** (2021), 3954–3967. https://doi.org/10.1109/TSMC.2019.2956121

23. F. Azlan, J. Kurnia, B. Tan, M. Z. Ismadi, Review on optimisation methods of wind farm array under three classical wind condition problems, *Renewable Sustainable Energy Rev.*, **135** (2021), 110047. https://doi.org/10.1016/j.rser.2020.110047

24. Y. Chen, H. Li, K. Jin, Q. Song, Wind farm layout optimization using genetic algorithm with different hub height wind turbines, *Energy Convers. Manage.*, **70** (2013), 56–65. https://doi.org/10.1016/j.enconman.2013.02.007

25. X. Ju, F. Liu, Wind farm layout optimization using self-informed genetic algorithm with information guided exploitation, *Appl. Energy*, **248** (2019), 429–445. https://doi.org/10.1016/j.apenergy.2019.04.084

26. X. Ju, F. Liu, L. Wang, W. J. Lee, Wind farm layout optimization based on support vector regression guided genetic algorithm with consideration of participation among landowners, *Energy Convers. Manage.*, **196** (2019), 1267–1281. https://doi.org/10.1016/j.enconman.2019.06.082

27. Z. Lei, S. Gao, Y. Wang, Y. Yu, L. Guo, An adaptive replacement strategy-incorporated particle swarm optimizer for wind farm layout optimization, *Energy Convers. Manage.*, **269** (2022), 116174. https://doi.org/10.1016/j.enconman.2022.116174

28. Z. Lei, S. Gao, Z. Zhang, H. Yang, H. Li, A chaotic local search-based particle swarm optimizer for large-scale complex wind farm layout optimization, *IEEE/CAA J. Autom. Sin.*, **10** (2023), 1168–1180. https://doi.org/10.1109/JAS.2023.123387

29. Y. Yu, T. Zhang, Z. Lei, Y. Wang, H. Yang, S. Gao, A chaotic local search-based LSHADE with enhanced memory storage mechanism for wind farm layout optimization, *Appl. Soft Comput.*, **141** (2023), 110306. https://doi.org/10.1016/j.asoc.2023.110306

30. H. Yang, S. Gao, Z. Lei, J. Li, Y. Yu, Y. Wang, An improved spherical evolution with enhanced exploration capabilities to address wind farm layout optimization problem, *Eng. Appl. Artif. Intell.*, **123** (2023), 106198. https://doi.org/10.1016/j.engappai.2023.106198

31. H. Long, P. Li, W. Gu, A data-driven evolutionary algorithm for wind farm layout optimization, *Energy*, **208** (2020), 118310. https://doi.org/10.1016/j.energy.2020.118310

32. W. Li, E. Özcan, R. John, Multi-objective evolutionary algorithms and hyper-heuristics for wind farm layout optimisation, *Renewable Energy*, **105** (2017), 473–482. https://doi.org/10.1016/j.renene.2016.12.022

33. F. Bai, X. Ju, S. Wang, W. Zhou, F. Liu, Wind farm layout optimization using adaptive evolutionary algorithm with monte carlo tree search reinforcement learning, *Energy Convers. Manage.*, **252** (2022), 115047. https://doi.org/10.1016/j.enconman.2021.115047

34. X. Yu, Y. Lu, Reinforcement learning-based multi-objective differential evolution for wind farm layout optimization, *Energy*, **284** (2023), 129300. https://doi.org/10.1016/j.energy.2023.129300

35. T. A. Qureshi, V. Warudkar, Wind farm layout optimization through optimal wind turbine placement using a hybrid particle swarm optimization and genetic algorithm, *Environ. Sci. Pollut. Res.*, **30** (2023), 77436–77452. https://doi.org/10.1007/s11356-023-27849-7

36. B. Morales-Castañeda, D. Zaldivar, E. Cuevas, F. Fausto, A. Rodríguez, A better balance in metaheuristic algorithms: Does it exist?, *Swarm Evol. Comput.*, **54** (2020), 100671. https://doi.org/10.1016/j.swevo.2020.100671

37. Z. Cai, X. Yang, M. Zhou, Z. H. Zhan, S. Gao, Toward explicit control between exploration and exploitation in evolutionary algorithms: A case study of differential evolution, *Inf. Sci.*, **649** (2023), 119656. https://doi.org/10.1016/j.ins.2023.119656

38. M. Qaraad, S. Amjad, N. K. Hussein, M. A. Farag, S. Mirjalili, M. A. Elhosseini, Quadratic interpolation and a new local search approach to improve particle swarm optimization: Solar photovoltaic parameter estimation, *Expert Syst. Appl.*, **236** (2024), 121417. https://doi.org/10.1016/j.eswa.2023.121417

39. J. Gao, Z. Wang, T. Jin, J. Cheng, Z. Lei, S. Gao, Information gain ratio-based subfeature grouping empowers particle swarm optimization for feature selection, *Knowledge-Based Syst.*, **286** (2024), 111380. https://doi.org/10.1016/j.knosys.2024.111380

40. Z. Zhang, Z. Lei, M. Omura, H. Hasegawa, S. Gao, Dendritic learning-incorporated vision transformer for image recognition, *IEEE/CAA J. Autom. Sin.*, **11** (2024), 539–541. https://doi.org/10.1109/JAS.2023.123978

41. Z. Wang, S. Gao, Z. Lei, M. Omura, An information-based elite-guided evolutionary algorithm for multi-objective feature selection, *IEEE/CAA J. Autom. Sin.*, **11** (2024), 264–266. https://doi.org/10.1109/JAS.2023.123810

42. M. Črepinšek, S. H. Liu, M. Mernik, Exploration and exploitation in evolutionary algorithms: A survey, *ACM Comput. Surv. (CSUR)*, **45** (2013), 1–33. https://doi.org/10.1145/2480741.2480752

43. P. Cai, Y. Zhang, T. Jin, Y. Todo, S. Gao, Self-adaptive forensic-based investigation algorithm with dynamic population for solving constraint optimization problems, *Int. J. Comput. Intell. Syst.*, **17** (2024), 5. https://doi.org/10.1007/s44196-023-00396-2

44. N. Li, L. Ma, T. Xing, G. Yu, C. Wang, Y. Wen, et al., Automatic design of machine learning via evolutionary computation: A survey, *Appl. Soft Comput.*, **143** (2023), 110412. https://doi.org/10.1016/j.asoc.2023.110412

45. Z. Lei, S. Gao, Z. Zhang, M. Zhou, J. Cheng, MO4: A many-objective evolutionary algorithm for protein structure prediction, *IEEE Trans. Evol. Comput.*, **26** (2022), 417–430. https://doi.org/10.1109/TEVC.2021.3095481

46. Y. Cui, W. Hu, A. Rahmani, Multi-robot path planning using learning-based artificial bee colony algorithm, *Eng. Appl. Artif. Intell.*, **129** (2024), 107579. https://doi.org/10.1016/j.engappai.2023.107579

47. K. Hippalgaonkar, Q. Li, X. Wang, J. W. Fisher III, J. Kirkpatrick, T. Buonassisi, Knowledge-integrated machine learning for materials: lessons from gameplaying and robotics, *Nat. Rev. Mater.*, **8** (2023), 241–260. https://doi.org/10.1038/s41578-022-00513-1

48. P. Manandhar, H. Rafiq, E. Rodriguez-Ubinas, Current status, challenges, and prospects of data-driven urban energy modeling: A review of machine learning methods, *Energy Rep.*, **9** (2023), 2757–2776. https://doi.org/10.1016/j.egyr.2023.01.094

49. D. Cheng, J. Li, L. Liu, J. Liu, T. D. Le, Data-driven causal effect estimation based on graphical causal modelling: A survey, *ACM Comput. Surv.*, **56** (2024), 1–37. https://doi.org/10.1145/3636423

50. S. Gao, M. Zhou, Z. Wang, D. Sugiyama, J. Cheng, J. Wang, et al., Fully complex-valued dendritic neuron model, *IEEE Trans. Neural Networks Learn. Syst.*, **34** (2023), 2105–2118. https://doi.org/10.1109/TNNLS.2021.3105901

51. Z. Qian, Y. F. Xie, S. Xie, MAR-GSA: Mixed attraction and repulsion based gravitational search algorithm, *Inf. Sci.*, **662** (2024), 120250. https://doi.org/10.1016/j.ins.2024.120250

52. Z. Lei, S. Gao, H. Hasegawa, Z. Zhang, M. Zhou, K. Sedraoui, Fully complex-valued gated recurrent neural network for ultrasound imaging, *IEEE Trans. Neural Networks Learn. Syst.*, **2023** (2023), 1–14. https://doi.org/10.1109/TNNLS.2023.3282231

53. S. Gao, M. Zhou, Y. Wang, J. Cheng, H. Yachi, J. Wang, Dendritic neuron model with effective learning algorithms for classification, approximation, and prediction, *IEEE Trans. Neural Networks Learn. Syst.*, **30** (2019), 601–604. https://doi.org/10.1109/TNNLS.2018.2846646

54. Y. Zhang, G. Chen, L. Cheng, Q. Wang, Q. Li, Methods to balance the exploration and exploitation in differential evolution from different scales: A survey, *Neurocomputing*, **561** (2023), 126899. https://doi.org/10.1016/j.neucom.2023.126899

55. Y. Yu, S. Gao, M. Zhou, Y. Wang, Z. Lei, T. Zhang, et al., Scale-free network-based differential evolution to solve function optimization and parameter estimation of photovoltaic models, *Swarm Evol. Comput.*, **74** (2022), 101142. https://doi.org/10.1016/j.swevo.2022.101142

56. Y. Yu, Z. Lei, Y. Wang, T. Zhang, C. Peng, S. Gao, Improving dendritic neuron model with dynamic scale-free network-based differential evolution, *IEEE/CAA J. Autom. Sin.*, **9** (2022), 99–110. https://doi.org/10.1109/JAS.2021.1004284

57. S. Gupta, S. Singh, R. Su, S. Gao, J. C. Bansal, Multiple elite individual guided piecewise search-based differential evolution, *IEEE/CAA J. Autom. Sin.*, **10** (2023), 135–158. https://doi.org/10.1109/JAS.2023.123018

58. R. Salgotra, A. H. Gandomi, A novel multi-hybrid differential evolution algorithm for optimization of frame structures, *Sci. Rep.*, **14** (2024), 4877. https://doi.org/10.1038/s41598-024-54384-3

59. Y. Yu, K. Wang, T. Zhang, Y. Wang, C. Peng, S. Gao, A population diversity-controlled differential evolution for parameter estimation of solar photovoltaic models, *Sustainable Energy Technol. Assess.*, **51** (2022), 101938. https://doi.org/10.1016/j.seta.2021.101938

60. A. V. Kononova, D. Vermetten, F. Caraffini, M. A. Mitran, D. Zaharie, The importance of being constrained: Dealing with infeasible solutions in differential evolution and beyond, *Evol. Comput.*, **32** (2024), 3–48. https://doi.org/10.1162/evco_a_00333

61. S. Gao, K. Wang, S. Tao, T. Jin, H. Dai, J. Cheng, A state-of-the-art differential evolution algorithm for parameter estimation of solar photovoltaic models, *Energy Convers. Manage.*, **230** (2021), 113784. https://doi.org/10.1016/j.enconman.2020.113784

62. S. Y. D. Sorkhabi, D. A. Romero, J. C. Beck, C. H. Amon, Constrained multi-objective wind farm layout optimization: Novel constraint handling approach based on constraint programming, *Renewable Energy*, **126** (2018), 341–353. https://doi.org/10.1016/j.renene.2018.03.053

63. R. Shakoor, M. Y. Hassan, A. Raheem, Y. K. Wu, Wake effect modeling: A review of wind farm layout optimization using Jensen's model, *Renewable Sustainable Energy Rev.*, **58** (2016), 1048–1059. https://doi.org/10.1016/j.rser.2015.12.229

64. G. Mosetti, C. Poloni, B. Diviacco, Optimization of wind turbine positioning in large windfarms by means of a genetic algorithm, *J. Wind Eng. Ind. Aerodyn.*, **51** (1994), 105–116. https://doi.org/10.1016/0167-6105(94)90080-9

65. S. Grady, M. Hussaini, M. M. Abdullah, Placement of wind turbines using genetic algorithms, *Renewable Energy*, **30** (2005), 259–270. https://doi.org/10.1016/j.renene.2004.05.007

66. A. M. Abdelsalam, M. El-Shorbagy, Optimization of wind turbines siting in a wind farm using genetic algorithm based local search, *Renewable Energy*, **123** (2018), 748–755. https://doi.org/10.1016/j.renene.2018.02.083

67. T. van der Beek, D. Souravlias, J. T. van Essen, J. Pruyn, K. Aardal, Hybrid differential evolution algorithm for the resource constrained project scheduling problem with a flexible project structure and consumption and production of resources, *Eur. J. Oper. Res.*, **313** (2024), 92–111. https://doi.org/10.1016/j.ejor.2023.07.043

68. Y. Liu, A. As'arry, M. K. Hassan, A. A. Hairuddin, H. Mohamad, Review of the grey wolf optimization algorithm: variants and applications, *Neural Comput. Appl.*, **36** (2024), 2713–2735. https://doi.org/10.1007/s00521-023-09202-8

69. K. C. Okafor, B. Adebisi, A. O. Akande, K. Anoh, Agile gravitational search algorithm for cyber-physical path-loss modelling in 5G connected autonomous vehicular network, *Veh. Commun.*, **45** (2024), 100685. https://doi.org/10.1016/j.vehcom.2023.100685

70. Y. Fu, M. Zhou, X. Guo, L. Qi, K. Gao, A. Albeshri, Multiobjective scheduling of energy-efficient stochastic hybrid open shop with brain storm optimization and simulation evaluation, *IEEE Trans. Syst. Man Cybern.: Syst.*, **54** (2024), 4260–4272. https://doi.org/10.1109/TSMC.2024.3376292

71. Z. Zhang, Q. Yu, H. Yang, J. Li, J. Cheng, S. Gao, Triple-layered chaotic differential evolution algorithm for layout optimization of offshore wave energy converters, *Expert Syst. Appl.*, **239** (2024), 122439. https://doi.org/10.1016/j.eswa.2023.122439

72. R. Zhong, E. Zhang, M. Munetomo, Evolutionary multi-mode slime mold optimization: a hyper-heuristic algorithm inspired by slime mold foraging behaviors, *J. Supercomput.*, **80** (2024), 12186–12217. https://doi.org/10.1007/s11227-024-05909-0

73. J. Li, M. H. Dao, Q. T. Le, Data-driven modal parameterization for robust aerodynamic shape optimization of wind turbine blades, *Renewable Energy*, **224** (2024), 120115. https://doi.org/10.1016/j.renene.2024.120115

74. R. Atha, A. Rajan, S. Mallick, An enhanced Equilibrium Optimizer for solving complex optimization problems, *Inf. Sci.*, **660** (2024), 120077. https://doi.org/10.1016/j.ins.2023.120077

75. Y. Cao, H. Zhang, W. Li, M. Zhou, Y. Zhang, W. A. Chaovalitwongse, Comprehensive learning particle swarm optimization algorithm with local search for multimodal functions, *IEEE Trans. Evol. Comput.*, **23** (2019), 718–731. https://doi.org/10.1109/TEVC.2018.2885075

76. Y. Wang, S. Gao, Y. Yu, Z. Cai, Z. Wang, A gravitational search algorithm with hierarchy and distributed framework, *Knowledge-Based Syst.*, **218** (2021), 106877. https://doi.org/10.1016/j.knosys.2021.106877

77. S. Karimkashi, A. A. Kishk, Invasive weed optimization and its features in electromagnetics, *IEEE Trans. Antennas Propag.*, **58** (2010), 1269–1278. https://doi.org/10.1109/TAP.2010.2041163

78. D. Wilson, S. Rodrigues, C. Segura, I. Loshchilov, F. Hutter, G. L. Buenfil, et al., Evolutionary computation for wind farm layout optimization, *Renewable Energy*, **126** (2018), 681–691. https://doi.org/10.1016/j.renene.2018.03.052